Eur. Phys. J. Special Topics **220**, 123–137 (2013)

DOI: 10.1140/epjst/e2013-01802-7

THE EUROPEAN PHYSICAL JOURNAL SPECIAL TOPICS

Review

Electromagnetic melt flow control during solidification of metallic alloys

Sven Eckert[1], Petr A. Nikrityuk[4], Bernd Willers[1], Dirk Räbiger[1], Natalia Shevchenko[1], Hieram Neumann-Heyme[2], Vadim Travnikov[2], Stefan Odenbach[2], Axel Voigt[3], and Kerstin Eckert[2]

[1] Helmholtz-Zentrum Dresden-Rossendorf (HZDR), Institute of Fluid Dynamics, 01314 Dresden, Germany
[2] Technische Universität Dresden (TUD), Institute of Fluid Mechanics, 01062 Dresden, Germany
[3] TUD, Institute for Scientific Computing, 01062 Dresden, Germany
[4] TU Bergakademie Freiberg, CIC Virtuhcon Department of Energy, Process- and Chemical Engineering, Fuchsmühlenweg 9, 09596 Freiberg, Germany

Received 16 January 2013 / Received in final form 5 February 2013
Published online 26 March 2013

Abstract. In this minireview, we summarize experimental and numerical studies particularly concerned with applications of rotating magnetic fields (RMF) or travelling magnetic fields (TMF) to directional solidification of metal alloys. After introducing some fundamentals of electromagnetic stirring, we review the insights gained into flow-induced modifications of microstructure and the formation of freckles and macrosegregations. We further discuss recent strategies, using time-modulated RMF and TMF, which aim to overcome the deficiencies of conventional stirring, in particular flow-induced macrosegregation, by effectively controlling the flow field. On the microscale, we show that time-varying flows are able to alter the sidebranch characteristics vital to the potential of fragmentation.

1 Introduction

In the majority of cases, solidification processes occur in the presence of melting bath movements. Because the effects of the melt flow are traceable in the structure, the interaction between convection and solidification became an important field of investigation. The formation of the microstructure can be intentionally influenced by mechanical or electromagnetic stirring. This forced convection promotes, among other things, an earlier transition from columnar to equiaxed, dendritic growth (CET) and provokes a distinct grain refining effect (see for instance [1–7]). However, melt flow during solidification can cause unwanted macrosegregation [8–12]. Despite a number of existing theoretical and experimental studies, considerable deficits remain regarding a comprehensive understanding of the mechanisms of interaction between convection in the liquid phase and solidification. However, such knowledge is a vital prerequisite for controlling solidification processes.

The goal of the research work conducted at HZDR and TUD is the application of tailored magnetic fields during solidification to efficiently create homogeneous, fine-grained, globular structures without macrosegregation. The focus is on electromagnetic stirring of the melt during solidification by AC magnetic fields. Solidification can also be influenced by DC magnetic fields, cf. [13]; in particular by high magnetic fields, see recent review [14], or by electric fields, e.g. [15,16]. However, such approaches are not considered here. We present a brief review devoted to the application of rotating or travelling magnetic fields for flow control in solidifying metal alloys. Generic model experiments were carried out on laboratory scale, which simplifies the problems and generates more information about physical relationships between structure formation and convection in solidification of metallic alloys.

2 Fluid flow during electromagnetic stirring

A flow in a solidifying, electrically conducting melt can be generated by applying time-varying magnetic fields. The most prominent realizations of them are induction coils [17] in furnaces and rotating [18,19] or travelling [5,12,20] magnetic fields. Such fields are a powerful tool to provide a wide variety of flow patterns through which the solidifying microstructure can be tailored in-situ. The application of electromagnetic fields for stirring the melt bath is attractive because they allow for (i) completely contactless influence on the molten metal, (ii) direct and simple control of the flow intensity through electric control parameters, and iii) flexible tailoring of the magnetic fields themselves, which can be combined and modulated at random to create any flow pattern required. While attempts to understand the flow fields underlying electromagnetic(em)-stirring go back to the 1980s [18–20], considerable progress has been made in the past ten years in particular for RMF and TMF-driven fluid flow by employing careful model experiments of low-melting-point alloys and adapted numerical simulations. A standard case to be considered here is the axisymmetric arrangement of a cylindrical liquid metal column exposed to an RMF or a TMF. In the steady state, the primary flow driven by an RMF is a rotation of the fluid around the cylinder axis. The Lorentz force is not uniform along the axial direction, but reaches a maximum at the horizontal midplane of the cylinder. Therefore, the fluid rotates faster here compared to the regions at the top and the bottom, where the velocity declines to zero at the wall across the developing Bödewadt boundary layers. The consequence is an imbalance of the centrifugal forces, driving a radial outward flow at the horizontal midplane. For reasons of continuity, a secondary circulation appears in the r-z plane, which has the form of two toroidal vortices. The TMF provides driving force components in the vertical and radial directions, resulting in a toroidal single vortex. The flow direction depends on the phase relation between the TMF coils and can easily be adjusted upwards or downwards along the side walls of the fluid container.

Applications of steady RMF or TMF, respectively, do not yield optimal results for the directional solidification process. Temperature measurements during the directional solidification of Al-Si alloys revealed a poor mixing efficiency by an RMF [21]. This finding supports Nikrityuk et al. [22] who showed that only highly turbulent RMF-driven flows with pronounced instabilities in form of Taylor-Görtler vortices ensure sufficient melt homogenization. However, the intense RMF-driven flows cause a strong inward flow along the solidification front which transports solute towards the axis of the sample where distinct segregation channels emerge. The TMF is more efficient in terms of mixing, but also tends to form extensive, flow-induced segregation zones. Thus, more sophisticated stirring concepts are required for efficient control of melt flow during solidification. Moreover, solidification is a transient process.

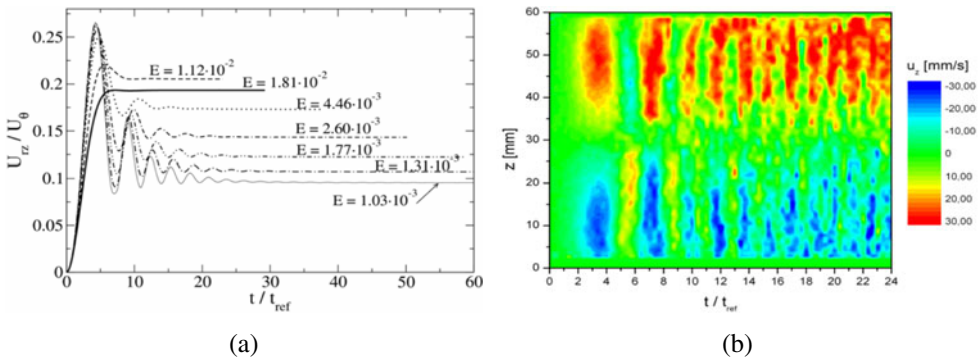

Fig. 1. History of the meridional flow field during an RMF-driven spin-up: (a) Numerical results of the volume-averaged meridional velocity for different values of the Ekman number E (from [23]); (b) Measurements of the flow profile of the vertical velocity along a vertical line at $r/R_0 = 0.9$ (from [27]).

The propagation of the solidification front permanently changes the ratio of liquid and solid region within the sample. Obviously, this fact has consequences for the Lorentz force and the resulting flow field. Therefore, studies concerning the impact of electromagnetically forced flow on solidification must consider the transient flow fields arising from non-stationary forcing. If an RMF is applied to a solidifying melt, an important step is the acceleration of the melt by the Lorentz force from a state of rest during the so-called spin-up process. For the sake of concision, we will only briefly discuss some important features of intermittently RMF-driven flows [23–27] and refer to other works for general descriptions of RMF and TMF-driven flows [28–30].

Numerical results with respect to the development of the secondary flow during an RMF-driven spin-up, represented by the volume-averaged meridional velocity, are plotted in Fig. 1(a) [23]. The first period of the spin-up, in which viscous effects play only a negligible role, is also called the initial adjustment phase and lasts until the first maximum of the curve. The nonlinear interaction between the primary and secondary flow becomes important in the subsequent inertial phase. The development of the secondary flow proceeds via inertial oscillations with the two-toroidal vortex pattern of the previous initial adjustment phase. As a result, the multilayered structure of the Bödewadt layers at the horizontal endwalls is established. For the supercritical values of the magnetic induction, Taylor-Görtler vortices appear near the sidewall layers and move from the horizontal midplane toward the horizontal endwalls, where they dissipate [23,27,31,32].

An interesting finding consists in recurring inversions of the direction of the secondary flow during the inertial phase of the RMF spin-up. This effect becomes obvious in the flow measurements presented in Fig. 1(b), which were carried out by Ultrasound Doppler Velocimetry inside a isothermal GaInSn melt [27]. The evolution of the vertical velocity near the side walls clearly shows the changeover of the meridional flow pattern. Such a flow structure appears to be very attractive for application during directional solidification, because it provides efficient homogenization of the temperature field in the melt and distinct temperature fluctuations adjacent to the solidification front. Both conditions are advantageous for increasing the number of nuclei in the melt and promoting equiaxed grain growth. Moreover, repeated reversals of the flow direction along the solidification front might be suitable to suppress flow-induced segregation, as discussed in Sect. 4 of this paper. This flow oscillations

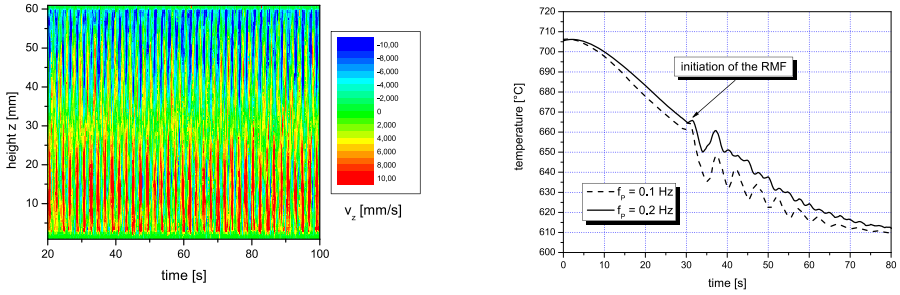

(a) (b)

Fig. 2. Excitation of an oscillatory secondary flow by a pulsed RMF: (a) spatio-temporal plot of the vertical velocity measured in GaInSn at a magnetic field of 5.8 mT and a pulse frequency of 0.475 Hz (from [33]); (b) Cooling curves obtained at the center of a cylindrical mold during the bottom-up solidification of an Al-7 wt%Si alloy.

can be maintained over a longer time period by the application of a time-modulated RMF, which can be realized, for instance, as a sequence of RMF-pulses. Figure 2(a) shows a spatio-temporal plot of the vertical velocity recorded in an isothermal GaInSn flow agitated by equidistant RMF-pulses [33]. A careful adjustment of the pulse frequency f_P is necessary in order to guarantee an intense secondary flow with periodic reversals of the flow direction. The optimum of f_P is associated with a selective inertial mode and depends on the magnetic field strength, the material properties of the melt, and the geometry of the problem [33]. A mismatch of the relevant parameters prevents an improvement of the mixing quality. Temperature measurements displayed in Fig. 2(b) verify the occurrence of this phenomenon for the solidification of Al-Si alloys. The thermocouple was situated in the center of the fluid vessel. The pulsed RMF was started with a time delay of 30 s after the onset of cooling. Distinct temperature oscillations can be observed, indicating a periodic up- and downwards flow which transports alternately hot and cold liquid along the sensor position. These oscillations are especially pronounced at a pulse frequency of 0.2 Hz, which almost coincides with the excitation frequency of an inertial mode under these experimental conditions. Section 4 presents results which demonstrate the capabilities of the time-modulated RMF to avoid flow-induced macrosegregation during the solidification of Al-Si alloys.

3 Flow-induced modifications of the microstructure

Grain orientation

A systematic measuring program considering the impact of RMF-driven flows on solidifying Pb-Sn and Al-Si alloys was conducted by the present authors. A detailed description of the experimental set-up can be found in [34]. The metal alloys were solidified directionally from the bottom in a cylindrical stainless steel mold. The mold has an internal diameter of 50 mm and a height of 100 mm. The filling height for each sample was 60 mm in the liquid state. The mold was positioned at a water-cooled copper chill, which was kept at a constant temperature of about 20 °C. To minimize radial heat transfer, the outer side wall was covered by heat insulation in the case of the Sn-Pb alloy, whereas a double-walled mold was used for processing the Al-Si alloys. A photograph showing the experimental setup is depicted in Fig. 3(a). The solidification experiments were performed at the COMMA (COMbined MAgnetic

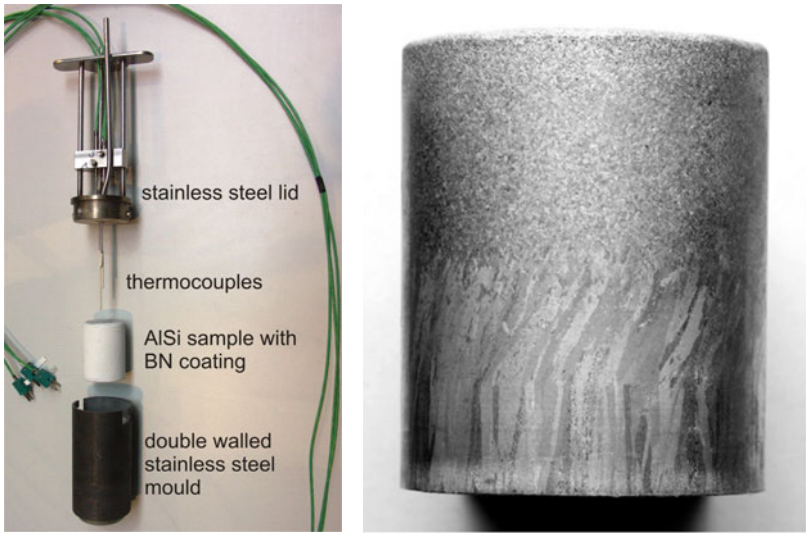

(a) (b)

Fig. 3. Solidification experiments at HZDR: (a) Photograph showing the mold, the solidified sample and the thermocouples for temperature measurements installed at the lid of the mold; (b) Macrostructure of a Pb-Sn sample on the lateral surface (from [35]).

field) facility of HZDR. The magnetic system allows for applications of both rotating and vertically travelling magnetic fields.

The experimental results reveal a distinct influence of electromagnetically-driven convection on the alignment of the grains, the CET and the grain size. Figure 3(b) shows examples of the macrostructure of Pb-Sn alloys from the lateral surface of the cylindrical samples. In this case solidification started without electromagnetic stirring. The magnetic field was turned on with a time offset of 60 sec after initiating mold cooling. At the begining, the columnar grains grow almost antiparallel to the heat flux. A tilting of the columnar grains towards the flow direction, which is clockwise here, can be noticed as soon as the forced flow is generated in the melt. This effect is known from previous investigations carried out in different experimental set-ups and different alloys [36–39]. Although the columnar structures exhibit an inclination towards the incident flow, no modification of the crystal orientation could be perceived by electron back scattering diffraction (EBSD) measurements [40]. The deflection of the growth direction of the columnar grains can be explained by the competing growth of primary and secondary arms in the direction of the incident flow. Murakami et al. [36] proposed such a mechanism to account for the fact that they found different deflection angles for columnar grains and columnar dendrites. Secondary arms oriented preferentially in the upstream direction may overgrow the neighboring primary arm on the upstream side. This secondary arm bears a tertiary arm which replaces the prior primary arm stopped behind it. Therefore, the columnar grain on the downstream side could grow at the expense of the one on the upstream side if the stopped dendrite is located along the upstream side of a grain boundary. Moreover, the melt flow causes a redistribution of the solute concentration around the growing dendrite, leading to a depletion in the upstream region and a corresponding accumulation of solute in the downstream zone. Accordingly, dendritic growth is promoted on the upstream side of the dendrite whereas a high solute concentration at the downstream side decelerates the growth, or even inhibit the formation of dendrite side arms. This explanation was confirmed by X-ray measurements in Ga-In alloys [41]. Also, phase-field simulations of free dendritic growth [42,43] document this phenomenon.

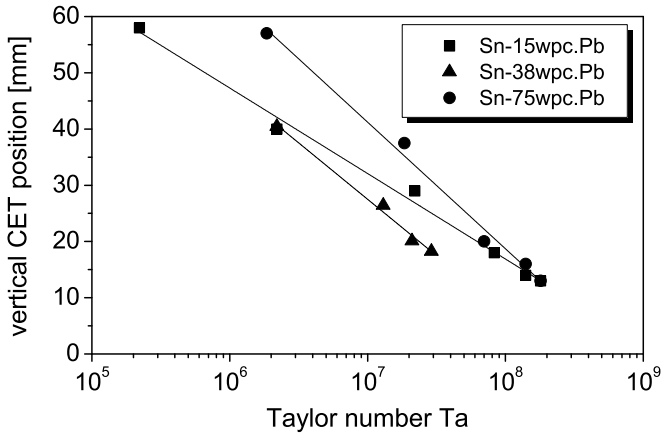

Fig. 4. Dependency of the vertical position of the CET on the magnetic Taylor number Ta (from [34]).

Columnar to equiaxed transition

The structure of castings generally shows different zones after solidification. A chill zone, where high cooling rates cause the development of many very small grains, is situated next to the wall of the mold, followed by a region where larger columnar dendrites occur. Finally, there is a certain probability that free nuclei existing in the area ahead of the progressing columnar front begin to grow and to form equiaxed dendrites. These crystallites either become stable or remelt, depending on the local thermal and solutal conditions. Often a qualitative transition of grain growth (CET) is observed at a certain point in time, when the columnar solidification front comes to a standstill. Now the subsequent solidified structure is shaped by a zone of equiaxed grains that is usually found in the center of a casting. There is a general consensus that the CET is determined by such process parameters as alloy system and composition, cooling rate, temperature gradient, pouring temperature, mold size, etc. The actual dependence on the individual parameters and the physical mechanism of the CET is still discussed controversial. For instance, Weinberg et al. [44,45] furnished proof of the CET in Pb-Sn and Al-Cu alloys when the temperature gradient ahead of the solidification front stays below a value critical to the associated material system, whereas Siqueira et al. [46] observed the CET for sufficiently low cooling rates. However, in view of the complexity of the process, a sole dependency on one single parameter can hardly be expected. Based on the evaluation of micrographs, some authors concluded that a CET occurs as soon as a critical number of equiaxed grains builds up ahead of the columnar front and physically blocks its advancement [47,48]. Another model focuses on the concentration field being affected by the equiaxed crystals [49]. Increased grain growth in the zone adjacent to the solidification front causes successive solute enrichment. Constitutional undercooling disappears, and the columnar dendrites ceases to grow. A melt flow provokes earlier occurrence of the CET [50]. The application of a TMF to the directional solidification of Al-Si alloys increases the area of equiaxed grains. The same finding was reported by the present authors for RMF-driven flow in Pb-Sn alloys [34,35]. As shown in Fig. 4, the vertical position of the CET can be shifted towards the bottom of the cylinder with increasing Taylor number Ta. This trend can be shown for different alloy compositions. In these experiments the CET occurs at a cooling rate of about 0.4 K/s and in the range between 0.6 and 1.0 K/mm for the temperature gradient. These critical values are about one order of magnitude higher than those found for the situation without forced

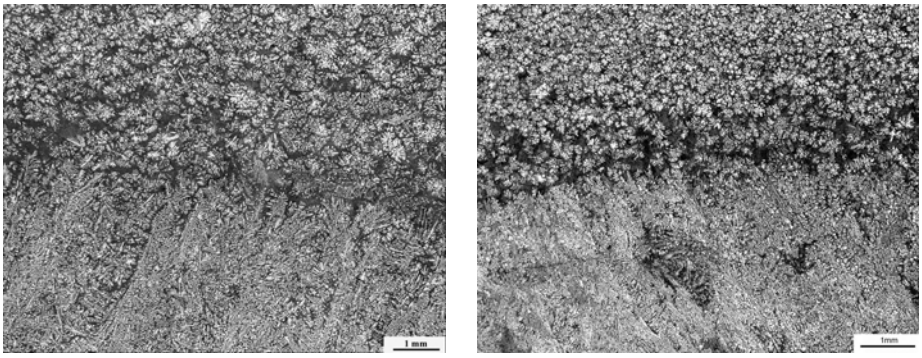

(a) (b)

Fig. 5. Micrographs showing the region where the CET occurs in Sn-15 wt%Pb alloys: (a) $B = 10$ mT; (b) $B = 20$ mT (from [34]).

convection [44,46]. Representative micrographs showing the dendritic structure in the CET region are displayed in Fig. 5. A strip containing a high amount of eutectic phase becomes visible along the columnar front. The higher concentration of solute in the CET region was confirmed by measurements of the phase distribution (not shown here). The accumulation of solute at the CET can be considered as the reason for the obstruction of further columnar growth in accordance with the concept of solutal blocking [49]. The source of nuclei for the equiaxed grains which finally stop the columnar growth may be either heterogeneous nucleation or a dendrite fragmentation process [51]. The issues of grain refinement and dendrite fragmentation will be discussed in the following paragraph.

Grain refinement and dendrite fragmentation

Various investigations have demonstrated that a pronounced decrease in grain size can be achieved with increasing intensity of forced convection in the solidifying melt [5,52–56]. For instance, the application of an RMF on solidifying Pb-Sn alloys provides grain refinement of both columnar and equiaxed grains [34,35]. Figure 6 shows the macrostructure of Al-Si alloys solidified in a cylindrical mold cooled from the side walls. The development of the mean grain size with the magnetic field strength can be seen in Fig. 7. It becomes obvious that the application of even small magnetic fields has a distinct influence on the grain size.

It is generally accepted that grain refinement in the absence of inocculants is caused by fragmentation of dendritic structures existing in the mushy zone [1], which has been observed in transparent model substances [57–59] and in metal alloys [60,61]. It seems plausible to attribute to the flow an active role in the formation of nuclei for equiaxed crystallization. Hellawell [51] suggests a mechanism of several steps:

1. The flow causes thermal and/or solutal fluctuations in the mushy zone, leading to a remelting of side arms from the dendritic network.
2. The flow transports these fragments from the interdendritic spacing to the region ahead of the solidification front.
3. In this area, characterized by a reduced temperature gradient, the fragments start to grow as equiaxed dendrites.
4. The advancing columnar solidification front stops as soon as the concentration of the equiaxed grains has reached a critical value.

In which way, however, does the flow cause fragmentation? Earlier research by Genders, among others [62] favored the picture of a mechanical smashing of dendrites

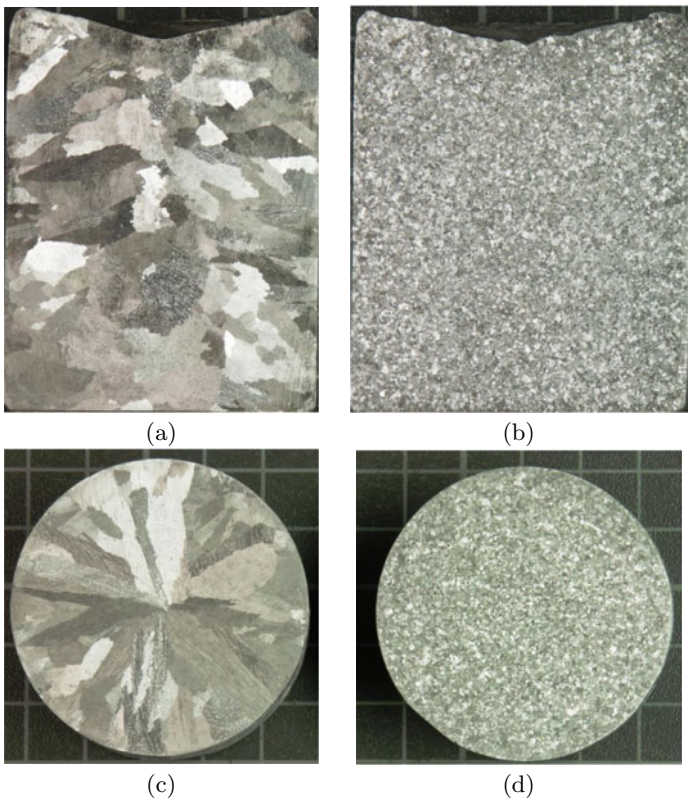

Fig. 6. Macrostructure of Al-7wt %Si alloys obtained from radial solidification (cooling from the side walls) without magnetic field (a,c) and under the influence of an RMF at $B = 9.2\,\mathrm{mT}$ (b,d). (a,b) show longitudinal and (c,d) horizontal cross-sections.

by the flow. Since [63], this mechanical fragmentation has not been considered important for grain refinement because the mechanical stresses acting in the dendrite neck remain far below the elasticity limit of the material. Currently, the preferred scenario is the remelting of the necks of individual dendrite arms [57]. This mechanism is based on the convective transport of solute and/or heat into the mushy zone. An alternative mechanism, called catastrophic elastic remelting, was recently proposed by [64], based on the idea that an elastic energy density affects the thermodynamic equilibrium at the solid-liquid interface. A further possibility is discussed by Hellawell [59], who traces the formation of dendrite fragments back to variations in growth velocity. Although the fluid flow acts on the fragmentation only via solute advection and fragment transport, oscillations of the flow velocity or liquid temperature may have a marked impact on sidebranch formation [65–67]. Figure 8 shows a 2D-phase field simulation in which either the velocity amplitude or the temperature of the parallel flow impinging the free dendrite, was modulated in time with a period t_p. The figure underlines that modulation with an optimal period of the pulses may lead to resonant sidebranching, by which a highly periodic array of sidebranches with elongated amplitudes can be achieved [67]. This work marks a first step towards understanding the influence of transient flow on growth conditions and sidebranch development, which itself is believed to be closely related to the potential of fragmentation. Regarding the flow impact onto other microstructural features, we refer to a recent review by Asta et al. [68].

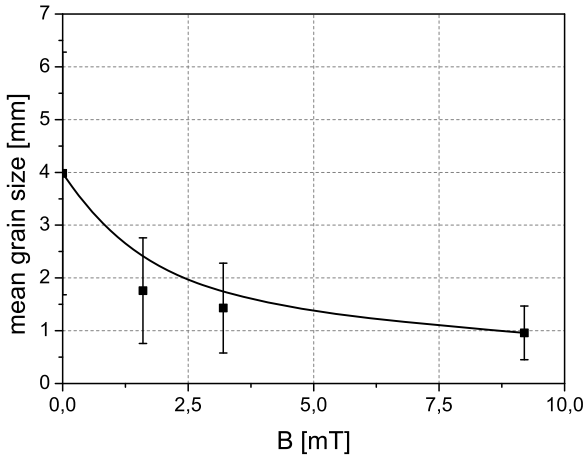

Fig. 7. Mean grain size as a function of the field strength of the RMF.

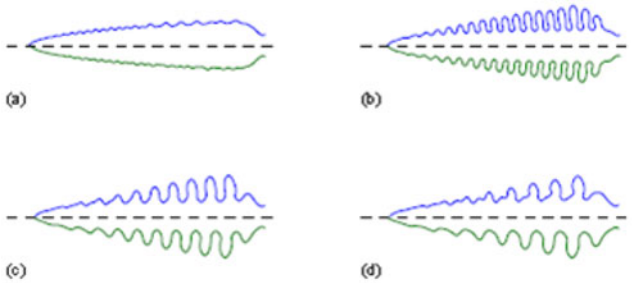

Fig. 8. Morphology of the streamwise facing dendrite branch at different ratios of the modulation period t_p to the resonant period t_{pr}: (a) $t_p/t_{pr} = 2/3$, (b) 1, (c) 5/3, (d) 2. Upper half in each picture: velocity modulation, lower half: temperature modulation [67].

4 Freckle formation and macrosegregations

Freckle

A characteristic flow-related defect at the borderline between micro- and macrostructure is the so-called freckle [69] which is frequently observed in ingots of several alloy systems. Freckles are channel-like segregations with geometrical dimensions of a few centimeters in length and several millimeters in width. There is a consensus that the occurrence of freckles is coupled to thermosolutal convection arising from unstable density stratification [70–72]. Since thermosolutal convection is modified by a forced convection, one can expect the freckle patterns to be changed by the application of AC magnetic fields. Indeed, Zaidat et al. [73] found a large central freckle at the bottom of a sample and hypothesized about TMF-induced recirculation loops penetrating the mushy zone such that a central upward flow exists. The location of such segregation channels was also studied in [12] for both RMF and TMF application. By comparing numerical computed flow patterns, they found a correlation between the stagnation points of the flow with the channel location.

However, detailed insight into how natural and forced convection interact with the microstructure during freckle formation was provided only recently by real-time X-ray observations at HZDR [41,74–76]. A series of directional bottom-up solidification experiments using the low-melting-temperature alloy Ga-25 wt%In were carried out at a cooling rate of 0.01 K/s accompanied by vertical temperature gradients in the

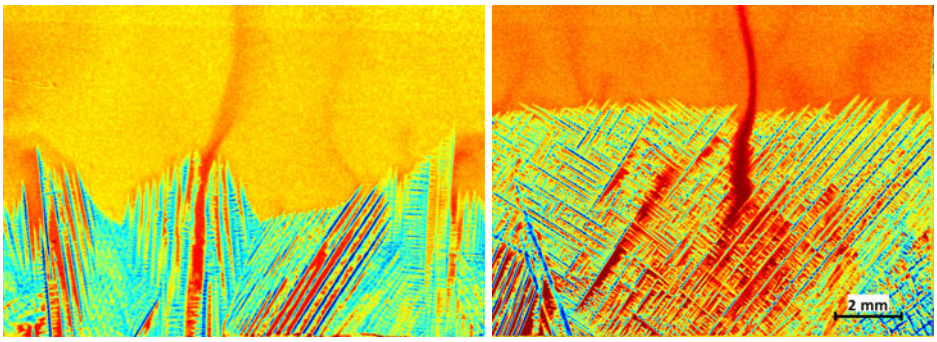

(a) (b)

Fig. 9. Image frames showing the dendritic network and segregation freckle formation at different temperature gradients: (a) 0.7–1 K/mm; (b) 2 K/mm.

range of 0.5 to 2 K/mm. Different formation of segregation channels were observed in the mushy zone that can be related to variations of the vertical temperature gradient. Solidifications carried out at temperature gradients up to 0.7–1 K/mm revealed the propagation of a corrugated solidification front and the formation of various segregation channels. Figure 9(a) shows a few strong jets of buoyant fluid, called plumes, in which the lighter Ga-rich melt (red areas) rises in front of blue In-2 wt%Ga dendrites during the early stage of the experiment. Later on, the plumes tend to both approach each other and merge. A dominating plume might be further intensified by the attraction of smaller neighboring plumes. The positions of the plumes are associated with individual fast-growing dendrites behind which they protrude from the growth front. However, not every initial segregation channel evolves into a stable chimney. Stable chimneys were observed in only 4 of 10 experiments and occur mainly at positions with initial growth defects or grain boundaries. The long-term stability of these segregation channels is strongly influenced by the transient nature of the melt convection.

The situation at higher temperature gradients (up to 2 K/mm) is characterized by two dominating convection rolls in the liquid phase, driven by a lateral temperature gradient, and the convex shape of the solidification front. The penetration of this flow pattern into the mushy zone results in a continuous accumulation of solute in the central part of the mushy zone followed by a remelting of the solid fraction and the occurrence of a stable chimney, see Fig. 9(b). In all solidification experiments performed under such conditions at least one stable chimney was detected. Thus the experiments show that initiation and development of the chimneys and their probability of surviving depends sensitively on the spatio-temporal structure of the flow field. Furthermore, variations of the vertical temperature gradient along the solidification cell lead to the observation of different mechanisms for chimney formation.

Macrosegregations

At sufficiently large values of the magnetic induction, electromagnetic stirring clearly dominates thermosolutal convection. However, this does not imply that the concentration distribution becomes homogeneous. On the contrary, characteristic macrosegregation patterns appear which are caused by the underlying flow structures. For an AlSi alloy directionally solidified in a cylindrical mold in presence of an RMF, [6] report on a top portion enriched in silicon and the peak in the eutectic fraction at the position of the CET. Similar channels on the axis [5,10–12], in which the silicon content is close to the eutectic composition, were also found in other works [10,12,77].

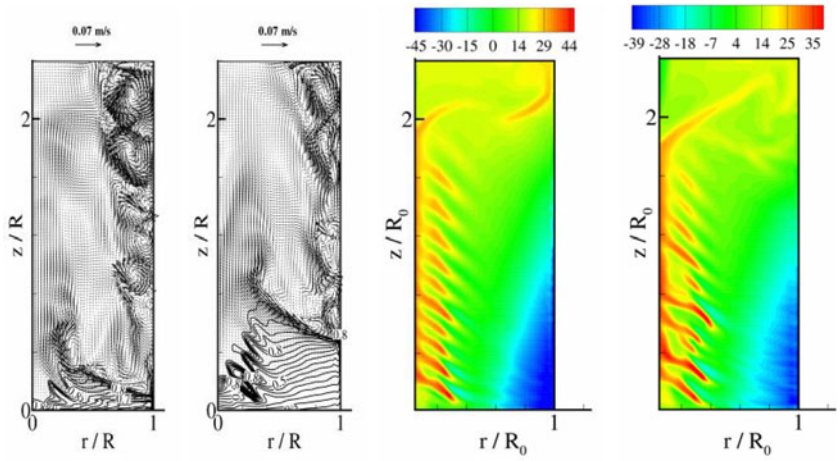

Fig. 10. Secondary flow driven by an RMF at 4 mT after 35 s (a) and 70 s (b) and the resulting macrosegregation patterns for B = 4 mT (c) and B = 2.5 mT (d) computed by using the K-model [77]. (c) and (d) show the relative concentration of silicon, $(C - C_0)/C_0$, in percent.

As in [6] we were able to attribute this phenomenon clearly to the secondary flow inside the liquid phase [11]. The vortex near the mushy zone carries solute which is rejected ahead of the mushy zone towards the central parts of the liquid phase. The advection of silicon-enriched liquid is responsible for the development of a liquid channel on the axis of rotation inside the mushy zone due to local remelting, which was also predicted in [78] for a laminar flow.

For even higher Taylor numbers larger than the critical Taylor number [79] at which the laminar flow loses its stability, the previous macrosegregation pattern is modified toward the so-called fir-tree pattern depicted in Fig. 10(c). In parallel, the velocity field of the secondary flow is plotted in Fig. 10(a,b) for two different times. The turbulent flow field is now characterized by randomly appearing Taylor-Görtler (T-G) vortices along the side wall of the cylinder. The T-G vortices are advected by the meridional flow toward the top and the mushy zone where they are dissipated. Figure 10(a,b) demonstrates a significant amplification of the radial flow, forming a jet along the mushy zone if the T-G vortex impinges there. As a consequence, the solute transport in the radial direction is momentarily enhanced. Local remelting occurs in spots with a particularly high silicon concentration near the axis, leading to a wavy shape of the mushy zone (Fig. 10). As a result, fir-tree segregation patterns exhibit characteristic side arm freckles. These findings are in good agreement with the experimental data [80]. Surprisingly, the fir-tree pattern becomes increasingly irregular with decreasing magnetic induction, cf. Fig. 10(d), because the frequency by which the T-G vortices hit the columnar front becomes smaller.

The structures of Fig. 10 were computed by using a permeability model out of the classes of mixture models originally introduced in [81]. Here, the mushy zone is treated as a porous medium, the permeability of which depends on the dendrite arm spacing and on the liquid fraction, see [77]. If significant advection of floating dendrites must be accounted for, an aspect not included in the K-model, a hybrid model [82] that switches between mixture viscosity and the permeability approach depending on the decreasing liquid fraction is a better choice. The resulting silicon

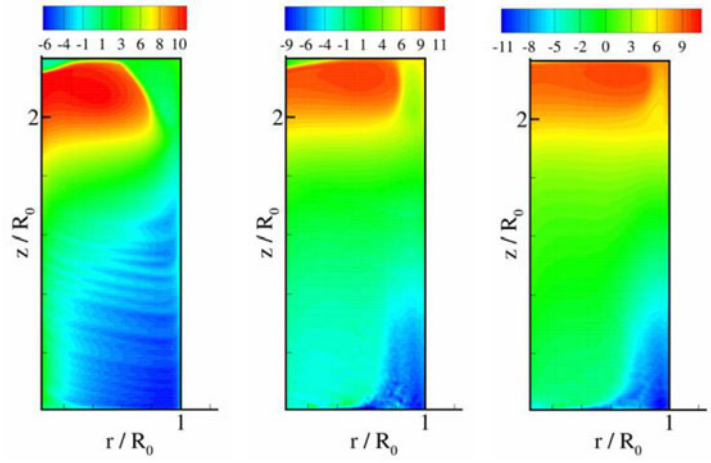

Fig. 11. Macrosegregation patterns in the RMF for B = 1 mT (a), B = 2.5 mT (b) and B = 4 mT (c) computed by using the hybrid model, which takes the motion of the equiaxed dendrites in the mushy zone into account [83]. Again, the relative silicon concentration, $(C - C_0)/C_0$, in percent is shown.

concentration is plotted in Fig. 11. We note that the final macrosegregation is considerably modified with respect to the columnar solidification. In particular, increasing the Taylor number decreases the macrosegregation in the middle and lower parts. The reason is seen in the T-G vortices appearing in the turbulent regime. They lead to enhanced mixing of the slurry of floating dendrites and solute-rich fluid with the bulk liquid. Furthermore, the transport of the floating dendrites by the flow reduces the 'wash' effect from the solid interface resulting from the advection of the rejected solute, in comparison with non-movable dendrites [83].

Macrosegrations in the TMF were studied e.g. in [12,84] and differ from those in the RMF. The distribution of the eutectic zones depends on the direction of the Lorentz force, e.g. for an downward-travelling magnetic field, counteracting solutal buoyancy, a certain reduction of macrosegregations can be achieved [85].

Nevertheless, solute accumulation cannot be suppressed during *continuous* stirring by either an RMF or TMF. A representative example of a pronounced segregation channel induced by a continuous RMF can be seen in Fig. 12. A promising route for control of macrosegregations was opened recently by the introduction of temporarily modulated magnetic fields [21,33,77,83,86,87]. The strategy for efficient modulation based on the insights into the flow structure is briefly discussed in Sect. 2. Further details can be found in [21,33]. Willers et al. [77] applied a pulsed RMF during the bottom-up solidification of Al-7 wt%Si alloys. The segregation at the axis, typical for an RMF, disappears completely for pulse frequencies $f_P > 0.3\,Hz$. Figure 13 presents measurements of the fraction of primary crystals across the horizontal cross-section of the solidified sample. As mentioned above, a remarkable enrichment of eutectic phase at the sample axis becomes apparent for the situation of a continuous RMF. The application of a pulsed RMF at a small pulse frequency diminishes the segregation marginally, whereas it disappears almost completely at higher frequencies. The alternating power up and power down of the magnetic field generates successive spin-ups and spin-downs of the rotating fluid flow. Abrupt changes in energy injection rates promote the propagation of inertial waves through the interior of the fluid.

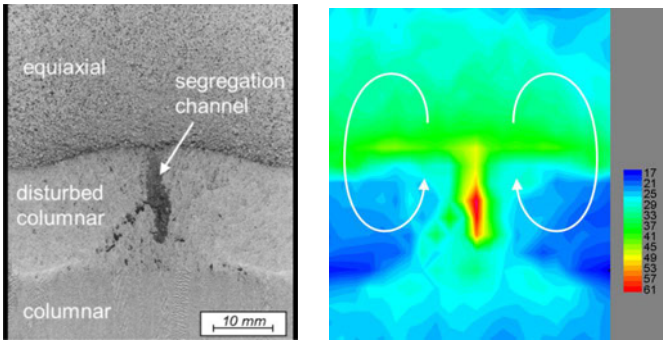

(a) (b)

Fig. 12. Flow-induced segregation pattern on the longitudinal section of a Sn-Pb alloy solidified under the influence of an RMF: (a) Macrostructure, (b) distribution of the eutectic phase.

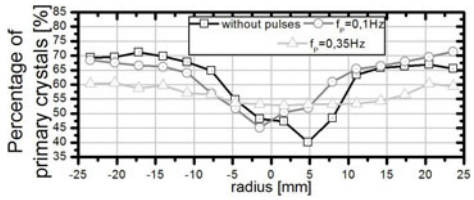

Fig. 13. Radial distribution of the surface area covered by primary crystals in an Al-7 wt%Si alloy solidified directionally from the bottom under the influence of continuous and pulsed RMFs, respectively.

The permanent reversals of the flow direction prevent any unidirectional transport of solute along the solidification front and, hence, hinder the formation of flow-induced segregation channels.

5 Summary

There is a wide agreement on the beneficial impact of rotating and travelling magnetic fields on solidifying melts, in the form of a stimulation of the CET and grain refinement. However, the drawbacks of conventional, continous electromagnetic stirring, consisting of flow-induced macrosegregations have also become apparent. Recent experimental and numerical results demonstrate the capabilities of subsequent pulses of an RMF and an upwards directed TMF to overcome this problem and also to prevent the formation of segregation freckles. But the problem of a targeted flow control during the solidification is complex because of the transient and turbulent flow and definitely requires further investigation. In addition, it remains unclear how the optimal flow structure for solidification looks like, and what kind of flow would promote the multiplication of nuclei in the melt to achieve equiaxed grain growth. For a better understanding of these questions, coordinated experimental and numerical studies of the interaction of flow fields with a columnar dendrite ensemble are highly desirable, including investigations of the processes of dendrite fragmentation and transport.

Financial support from Deutsche Forschungsgemeinschaft (DFG) in frame of the Collaborative Research Center (SFB) 609, Projects B1, B2 and C10 is gratefully acknowledged.

References

1. M. Flemings, Metall. Trans. B **22**, 269 (1991)
2. W. Johnston, G. Kotler, S. Ohara, H. Ashcom, W. Tiller, AIME Met. Soc. Trans. **233**, 1856 (1965)
3. S. OHara, W. Tiller, Trans. Met. Soc. AIME **239**, 497 (1967)
4. C. Vives, Int. J. Heat Mass Transfer **33**, 2585 (1990)
5. W. Griffiths, D. McCartney, Mater. Sci. Eng.: A **216**, 47 (1996)
6. J. Roplekar, J. Dantzig, Int. J. Cast Metals Res. **14**, 79 (2001)
7. G. Zimmermann, A. Weiss, Z. Mbaya, Mater. Sci. Eng. A **413–414**, 236 (2005)
8. C. Beckermann, Int. Mater. Rev. **47**, 243 (2002)
9. M. Medina, Y. Terrail, F. Durand, Y. Fautrelle, Metall. Mater. Trans. B **35**, 743 (2004)
10. S. Steinbach, L. Ratke, Metall. Mater. Trans. A **38**, 1388 (2007)
11. P. Nikrityuk, K. Eckert, R. Grundmann, Int. J. Heat Mass Transfer **49**, 1501 (2006)
12. A. Noeppel, A. Ciobanas, X. Wang, K. Zaidat, N. Mangelinck, O. Budenkova, A. Weiss, G. Zimmermann, Y. Fautrelle, Metall. Mater. Trans. B **41**, 193 (2010)
13. P. Nikrityuk, K. Eckert, R. Grundmann, Metall. Mater. Trans. B **40**, 317 (2009)
14. Z. Sun, M. Guo, J. Vleugels, O.V. der Biest, B. Blanpain, Curr. Opinion Solid State Mater. Sci. **16**, 254 (2012)
15. P. Nikrityuk, S. Ananiev, K. Eckert, R. Grundmann, Magnetohydrodynamics **45**, 407 (2009)
16. P. Nikrityuk, K. Eckert, R. Grundmann, Y. Yang, Steel Res. Int. **78**, 413 (2007)
17. T. Campanella, C. Charbon, M. Rappaz, Scripta Materialia **49**, 1029 (2003)
18. K.H. Spitzer, M. Dubke, K. Schwerdtfeger, Metall. Trans. B **17**, 119 (1986)
19. J.L. Meyer, F. Durand, R. Ricou, C. Vives, Metall. Trans. B **15**, 471 (1984)
20. M. Dubke, K.H. Tacke, K.H. Spitzer, K. Schwerdtfeger, Metall. Trans. B **19**, 581 (1988)
21. D. Räbiger, M. Leonhardt, S. Eckert, G. Gerbeth, IOP Conf. Ser.: Mater. Sci. Eng. **27**, 012053 (2012)
22. P. Nikrityuk, K. Eckert, R. Grundmann, Metall. Mater. Trans. B **41**, 94 (2010)
23. P. Nikrityuk, M. Ungarish, K. Eckert, R. Grundmann, Phys. Fluids **17**, 067101 (2005)
24. P. Nikrityuk, K. Eckert, R. Grundmann, Acta Mechanica **186**, 17 (2006)
25. P. Nikrityuk, K. Eckert, R. Grundmann, Metall. Mater. Trans. B **37**, 349 (2006)
26. P. Nikrityuk, S. Eckert, K. Eckert, Eur. J. Mechanics-B/Fluids **27**, 177 (2008)
27. D. Räbiger, S. Eckert, G. Gerbeth, Exper. Fluids **48**, 233 (2010)
28. J. Stiller, K. Koal, W. Nagel, J. Pal, A. Cramer, Eur. Phys. J. Special Topics **220**, 111 (2013)
29. I. Grants, G. Gerbeth, Eur. Phys. J. Special Topics **220**, 215 (2013)
30. A. Cramer, J. Pal, G. Gerbeth, Eur. Phys. J. Special Topics **220**, 259 (2013)
31. J. Stiller, K. Fraňa, A. Cramer, Phys. Fluids **18**, 074105 (2006)
32. T. Vogt, I. Grants, D. Räbiger, S. Eckert, G. Gerbeth, Exper. Fluids **52**, 1 (2012)
33. S. Eckert, P. Nikrityuk, D. Räbiger, K. Eckert, G. Gerbeth, Metall. Mater. Trans. B **39**, 374 (2008)
34. B. Willers, S. Eckert, U. Michel, I. Haase, G. Zouhar, Mater. Sci. Eng. A **402**, 55 (2005)
35. S. Eckert, B. Willers, P. Nikrityuk, K. Eckert, U. Michel, G. Zouhar, Mater. Sci. Eng. A **413**, 211 (2005)
36. K. Murakami, T. Fujiyama, A. Koike, T. Okamoto, Acta Metall. **31**, 1425 (1983)
37. K. Murakami, H. Aihara, T. Okamoto, Acta Metall. **32**, 933 (1984)
38. S. Lee, S. Lee, C. Hong, ISIJ International **40**, 48 (2000)
39. A. Turchin, D. Eskin, L. Katgerman, Mater. Sci. Eng. A **413**, 98 (2005)
40. S. Eckert, D.Räbiger, M. Mathes, G. Zimmermann, E. Schaberger-Zimmermann, IOP Conf. Ser.: Mater. Sci. Eng. **27**, 012051 (2012)
41. S. Boden, S. Eckert, G. Gerbeth, Mater. Lett. **64**, 1340 (2010)
42. X. Tong, C. Beckermann, A. Karma, Q. Li, Phys. Rev. E **63**, 061601 (2001)
43. Y. Lu, C. Beckermann, J. Ramirez, J. Crystal Growth **280**, 320 (2005)
44. R. Mahapatra, F. Weinberg, Metall. Trans. B **18**, 425 (1987)
45. I. Ziv, F. Weinberg, Metall. Trans. B **20**, 731 (1989)
46. C. Siqueira, N. Cheung, A. Garcia, Metall. Mater. Trans. A **33**, 2107 (2002)

47. J. Hunt, Mater. Sci. Eng. **65**, 75 (1984)
48. H. Fredriksson, Metall. Trans. **3**, 2989 (1972)
49. M. Martorano, C. Beckermann, C.A. Gandin, Metall. Mater. Trans. A **34**, 1657 (2003)
50. G. Cole, G. Bolling, AIME Met. Soc. Trans. **236**, 1366 (1966)
51. A. Hellawell, S. Liu, S. Lu, JOM J. Minerals, Metals Mater. Soc. **49**, 18 (1997)
52. T. Campanella, C. Charbon, M. Rappaz, Metall. Mater. Trans. A **35**, 3201 (2004)
53. S. Nafisi, D. Emadi, M. Shehata, R. Ghomashchi, Mater. Sci. Eng. A **432**, 71 (2006)
54. F. Robles Hernandez, J. Sokolowski, J. Alloys Compounds **426**, 205 (2006)
55. D. Lu, Y. Jiang, G. Guan, R. Zhou, Z. Li, R. Zhou, J. Mater. Proc. Technol. **189**, 13 (2007)
56. Z. Chen, X. Wen, C. Chen, J. Alloys Compounds **491**, 395 (2010)
57. K. Jackson, J. Hunt, D. Uhlmann, T. Seward, Trans. Metall. Soc. AIME **236**, 149 (1966)
58. C. Paradies, M. Glicksman, R. Smith, S. Guceri, *Convective Effects on Dendrite Remelting in Mushy Zones*, in *Transport Phenomena in Food Processing*, First International Conference Proceedings (1992), p. 266
59. A. Hellawell, Modeling of Casting, Welding and Advanced Solidification Processes VII 565 (1995)
60. D. Ruvalcaba, R. Mathiesen, D. Eskin, L. Arnberg, L. Katgerman, Acta Mater. **55**, 4287 (2007)
61. S. Boden, B. Willers, S. Eckert, G. Gerbeth, Int. J. Cast Metals Res. **22**, 30 (2009)
62. R. Genders, *The Interpretation of the Macrostructure of Cast Metals* (Institute of Metals, 1926)
63. J. Pilling, A. Hellawell, Metall. Mater. Trans. A **27**, 229 (1996)
64. S. Ananiev, P. Nikrityuk, K. Eckert, Acta Mater. **57**, 657 (2009)
65. P. Bouissou, B. Perrin, P. Tabeling, Phys. Rev. A **40**, 509 (1989)
66. H. Neumann-Heyme, K. Eckert, S. Odenbach, IOP Conf. Ser.: Mater. Sci. Eng. **27**, 012045 (2012)
67. H. Neumann-Heyme, K. Eckert, A. Voigt, S. Odenbach, IOP Conf. Ser.: Mater. Sci. Eng. **33**, 012106 (2012)
68. M. Asta, C. Beckermann, A. Karma, W. Kurz, R. Napolitano, M. Plapp, G. Purdy, M. Rappaz, R. Trivedi, Acta Mater. **57**, 941 (2009)
69. A. Giamei, B. Kear, Metall. Trans. **1**, 2185 (1970)
70. R. McDonald, J. Hunt, Metall. Trans. **1**, 1787 (1970)
71. S. Copley, A. Giamei, S. Johnson, M. Hornbecker, Metall. Trans. **1**, 2193 (1970)
72. J. Sarazin, A. Hellawell, Metall. Trans. A **19**, 1861 (1988)
73. K. Zaidat, T. Ouled-Khachroum, G. Vian, C. Garnier, N. Mangelinck-Noël, M. Dupouy, R. Moreau, J. Crystal Growth **275**, e1501 (2005)
74. N. Shevchenko, S. Eckert, S. Boden, G. Gerbeth, IOP Conf. Ser.: Mater. Sci. Eng. **33**, 012035 (2012)
75. N. Shevchenko, S. Boden, S. Eckert, G. Gerbeth, IOP Conf. Ser.: Mater. Sci. Eng. **27**, 012085 (2012)
76. N. Shevchenko, S. Boden, S. Eckert, D. Borin, M. Heinze, S. Odenbach, Eur. Phys. J. Special Topics **220**, 63 (2013)
77. B. Willers, S. Eckert, P. Nikrityuk, D. Räbiger, J. Dong, K. Eckert, G. Gerbeth, Metall. Mater. Trans. B **39**, 304 (2008)
78. M. Hainke, J. Friedrich, G. Müller, J. Mater. Sci. **39**, 2011 (2004)
79. I. Grants, G. Gerbeth, J. Fluid Mech. **431**, 407 (2001)
80. J. Kovács, A. Rónaföldi, G. Gergely, Z. Gácsi, A. Roósz, 5th Decennial International Conference on Solidification Processing (Sheffield, England, 2007), p. 405
81. W. Bennon, F. Incropera, Int. J. Heat Mass Transfer **30**, 2161 (1987)
82. C. Oldenburg, F. Spera, Numer. Heat Transfer, Part B Fund. **21**, 217 (1992)
83. P. Nikrityuk, K. Eckert, S. Eckert, Int. J. Cast Metals Res. **22**, 236 (2009)
84. P. Prescott, F. Incropera, J. Heat Transfer **117** (1995)
85. P.J. Prescott, F.P. Incropera, D.R. Gaskell, Exper. Heat Transfer **9**, 105 (1996)
86. S. Eckert, P. Nikrityuk, D. Räbiger, B. Willers, K. Eckert, Int. J. Cast Metals Res. **22**, 78 (2009)
87. X. Wang, Y. Fautrelle, J. Etay, R. Moreau, Metall. Mater. Trans. B **40**, 82 (2009)